Inorganic Chemistry

Article

pubs.acs.org/IC

Compressed Cesium Polyhydrides: Cs^+ Sublattices and H_3^- Three-Connected Nets

Andrew Shamp, James Hooper, and Eva Zurek*

Department of Chemistry, State University of New York at Buffalo, Buffalo, New York 14260-3000, United States

Supporting Information

ABSTRACT: The cesium polyhydrides (CsH_n, $n > 1$) are predicted to become stable, with respect to decomposition into CsH and H_2, at pressures as low as 2 GPa. The CsH_3 stoichiometry is found to have the lowest enthalpy of formation from CsH and H_2 between 30 and 200 GPa. Evolutionary algorithms predict five distinct, mechanically stable, nearly isoenthalpic CsH_3 phases consisting of H_3^- molecules and Cs^+ atoms. The H_3^- sublattices in two of these adopt a hexagonal three-connected net; in the other three the net is twisted, like the silicon sublattice in the α-$ThSi_2$ structure. The former emerge as being metallic below 100 GPa in our screened hybrid density functional theory calculations, whereas the latter remain insulating up to pressures greater than 250 GPa. The Cs^+ cations in the most-stable $I4_1/amd$ CsH_3 phase adopt the positions of the Cs atoms in Cs-IV, and the H_3^- molecules are found in the (interstitial) regions which display a maximum in the electron density.

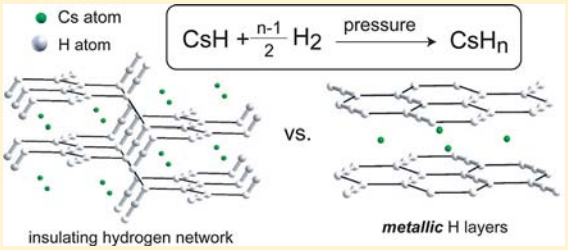

INTRODUCTION

Significant experimental effort has been devoted toward achieving pressure-induced metallization of hydrogen,[1−4] at times with controversial results.[5] The quest for the metallic allotrope of the lightest element is fueled by the prediction that it may be a high-temperature superconductor. Indeed, the SCDFT (DFT for superconductors[6]) approach has found the *Cmca* phase—predicted using the *ab initio random structure searching* (AIRSS) method[7]—to have a critical temperature (T_c) of up to 240 K at 450 GPa.[8] AIRSS computations have been used to search for the most likely structures of hydrogen up to 5 TPa,[9] and the atomic form that was found to be the most stable near 1.5 TPa was calculated to have a T_c as high as 764 K.[10] Recently, the particle swarm optimization technique[11] has uncovered new phases of hydrogen at TPa pressures.[12]

Another approach which may ultimately lead toward the metallization of hydrogen at experimentally achievable pressures is doping with an impurity.[13−15] Computations have predicted metallicity and superconductivity in hydrogen-rich compounds such as GeH_4,[16] SnH_4,[17,18] PbH_4,[19] GaH_3,[20] CaH_6,[21] and various MH_3 hydrides.[22] The theoretical predictions of metallic hydrogen-rich phases, and experimental studies of systems with nontraditional stoichiometries such as $Xe-H_2$,[23] SiH_4-H_2,[24−27] and H_2S-H_2[28] have inspired us to theoretically examine the structures of the alkali-metal polyhydrides under pressure.

Our computations have shown that LiH_n,[29] NaH_n,[30] KH_n,[31] and RbH_n,[32] where $n > 1$, become stable with respect to decomposition into hydrogen and the traditional alkali hydrides at 100, 25, 3, and 2 GPa, respectively. The pressure at which stabilization occurs is correlated with the ionization potential of the metal. No straightforward relationship could be found between the stoichiometries of the most stable polyhydride throughout the majority of the pressure range considered—LiH_6, NaH_9, KH_5, RbH_5—and the ionic radius. However, the pressure-induced symmetrization of H_3^- molecules in KH_5, RbH_5, and RbH_3, and their absence in the lithium and sodium polyhydrides, was shown to be related to the softness of the cation.[31] The interaction of a H^- base with a weak acid like H_2 to form H_3^- occurs most easily under pressure in the presence of the softest acid, because the strength of the cation/H^- interactions affects the H_2/H^- interactions. Since Li^+ and Na^+ are harder acids, symmetric H_3^- units may not form under pressure and, indeed, the most stable species were found to contain H^- or $H_2^{(-2/n)}$ entities.

Since Cs has an ionization potential comparable to that of Rb, one would expect that about the same amount of compression is required to stabilize CsH_n ($n > 1$) as their lighter cousins. In addition, because Cs is an even softer acid, it is likely that the preferred structures contain H_3^- units that become symmetric at even lower pressures than in RbH_5. In order to test these predictions, we have employed the evolutionary algorithm (EA) XtalOpt[33,34] to search for the most stable cesium polyhydride phases under pressure. Unsurprisingly, our hypotheses are confirmed. What we find remarkable, however, is the existence of five nearly isoenthalpic CsH_3 phases whose Cs^+ and H_3^- sublattices are reminiscent of the thorium sublattices and silicon three-connected nets found in the two known allotropes of $ThSi_2$. Perhaps even more fascinating is the observation that the most stable phase throughout a majority of the pressure range, $I4_1/amd$ CsH_3, can be constructed by placing H_3^- units in the regions where the

Received: May 19, 2012
Published: August 16, 2012

   dx.doi.org/10.1021/ic301045v | *Inorg. Chem.* 2012, 51, 9333−9342

electrons are found in Cs-IV, which has previously been considered as an electride (Cs^+e^-).[35]

■ ENTHALPIC TRENDS

The computed enthalpies of formation, ΔH_F, of the most favorable CsH_n (n = 2–9, 16) structures found in our evolutionary runs are provided in Figure 1. Exploratory

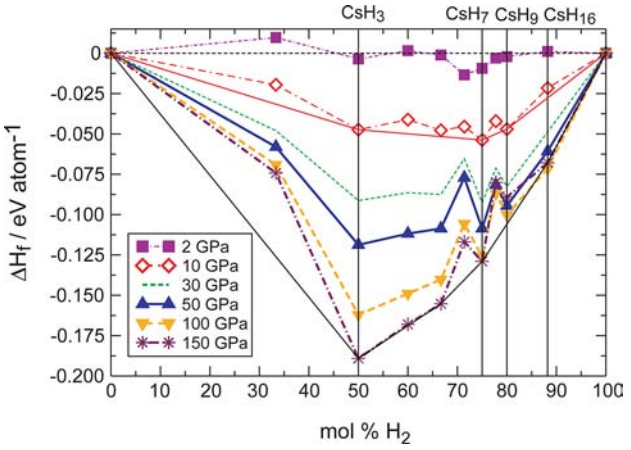

Figure 1. ΔH_F for the reaction $CsH + {}^1/_2(H_2)_{n-1} \rightarrow CsH_n$ versus the H_2 composition at various pressures. The enthalpies of CsH and H_2 are computed for the most stable structures from refs 36 and 37, and ref 7, respectively. The red and black solid lines represent the convex hulls at 10 and 150 GPa.

calculations indicated that phases with n = 10–15 correspond to thermodynamically unstable species in the hydrogen-rich region of the Cs–H phase diagram, so they were not examined further. We find the cesium polyhydrides start to become viable with respect to decomposition into CsH and H_2 at about 2 GPa. The rubidium polyhydrides became preferred at roughly the same pressure, which is consistent with the nearly equivalent ionization potentials of the two alkali metals: 3.9 vs 4.2 eV, respectively.

In order to determine which structures and stoichiometries could potentially be synthesized in high-pressure experiments, tie-lines were drawn between the ΔH_F of the various phases. The convex hull can be constructed by finding those points that do not fall below lines connected to it on either side.[38] Provided that they do not exhibit any unstable phonon modes, the phases on the convex hull are thermodynamically stable, whereas those above it are metastable. CsH_3, CsH_4, CsH_5, CsH_7, CsH_9, and CsH_{16} were all found to lie on the convex hull at some pressure within the 2–150 GPa range, as illustrated in Figure 1.

Between 2 and ~30 GPa, CsH_7 had the most negative ΔH_F out of all of the structures that we examined. However, CsH_3 became the most stable polyhydride above 30 GPa and remained so until at least 150 GPa. At pressures greater than 150 GPa, the magnitude of the enthalpy of formation starts to decrease, instead of continuing to increase, for most of the stoichiometries considered (see the Supporting Information, SI). Although EA calculations at these pressures were not performed, these trends follow those observed in rubidium polyhydrides under pressure.[32] Thus, it is likely that even CsH_3, for which ΔH_F (150 GPa) $\simeq$ ΔH_F (200 GPa), will start to become destabilized, with respect to CsH and H_2, at sufficiently high pressures.

The structural motifs present in the cesium polyhydrides depend on the pressure and the stoichiometry. The configurations found in our evolutionary runs can be classified as being composed of one of the following: (1) Cs^+ cations, H_2 molecules, and hydridic H^- anions; (2) Cs^+, H^-, and bent H_3^- molecules; (3) Cs^+, H_2, and H_3^-; and (4) Cs^+ and H_3^-. These groups are similar to those previously noted in compressed KH_n[31] and RbH_n.[32] For small n, the most favorable CsH_n geometries often contained a linear H_3^- molecule, whereas the likelihood of the presence of only H_2 molecules and a hydridic H^- anion was found to increase for n > 5. On the other hand, the hydrogenic sublattice in the lithium[29] or calcium polyhydrides[21] consisted of H_2 molecules with slightly stretched bonds and/or H^- units. The presence of the latter was only observed in systems for which the number of "effectively added electrons" (EAE) per H_2, and therefore the filling of the σ^* bands, was large.[21] Other pressure-stabilized phases, whose electronic structures can be understood by considering the electronegativity differences between the atoms, include Li_7Cs,[39] Li_5H,[40] or K–Ag intermetallics.[41]

■ $H^-\cdots H_2$ CONTACTS IN CsH_7

The stoichiometry with the most negative ΔH_F throughout a pressure range of ~2–30 GPa, CsH_7, was found to possess $P4/nmm$ symmetry. Its structure may be described as a body-centered cubic (bcc) lattice of hydrogens with half of the central positions occupied by Cs^+ cations. Most of the H_2 molecules lie on the eight corners of the cube, as illustrated in Figure 2a. The hydrogenic sublattice consists primarily of H_2 units whose bonds measure 0.776 Å at 50 GPa; these all point toward a single hydridic hydrogen near the vacant central positions, giving rise to numerous $H^-\cdots H_2$ contacts. The remaining H_2 molecules are also located near the vacant body

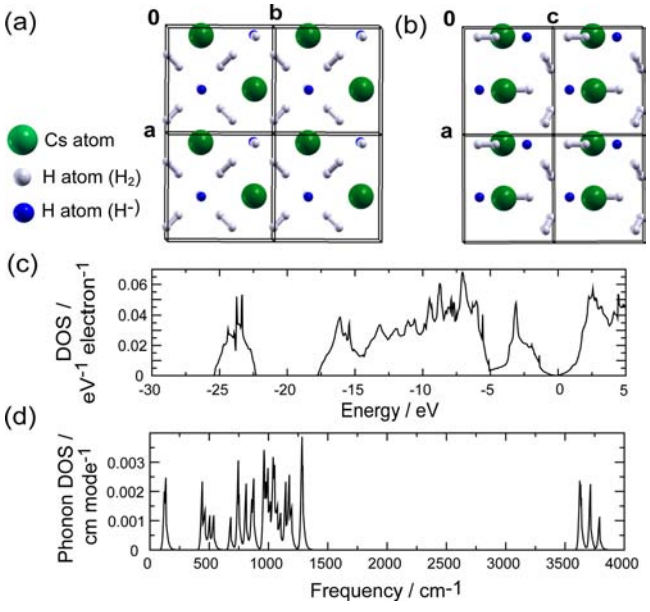

Figure 2. Two views of $P4/nmm$ CsH_7, where the Cs^+, H^-, and H_2 are colored as green, blue, and white, respectively. The first (a) shows the bcc-like lattice with Cs lying at the body center, and H_2 at the corners. The second (b)—formed from a rotation about the a-axis by 90°—illustrates the $H^-\cdots H_2$ configuration. The (c) electronic densities of states (DOS) at 100 GPa, and (d) phonon densities of states at 50 GPa of $P4/nmm$ CsH_7. The Fermi level has been set to zero.

dx.doi.org/10.1021/ic301045v | Inorg. Chem. 2012, 51, 9333–9342

centered positions such that they form a $H^-\cdots H_2$ arrangement that is notably shorter than the rest. While neither the H_2 molecule nor the H^- atom are located squarely in the body-centered position, the resulting $H^-\cdots H_2$ contact is; these motifs have a secondary effect of distorting the lattice's underlying cubes into rectangular parallelepipeds in order to encapsulate them (Figure 2b). This structural component is the first hint of the formation of an H_3^- molecule in CsH_n under pressure, but in CsH_7 a symmetric H_3^- is never formed up to 150 GPa. Even at 100 GPa, the intramolecular H−H distance (0.777 Å) is much shorter than the shortest $H^-\cdots H_2$ measure of 1.237 Å. Perhaps symmetrization does not occur because of the competition between multiple H_2 molecules that surround the H^-. This geometry is representative of many of the CsH_n structures with $n > 4$ found in our evolutionary searches.

The electronic densities of states at the PBE−metallization pressure in Figure 2c is indicative of substantial core overlap, which is consistent with previous results for the potassium and rubidium polyhydrides. The Cs 5s bands located near −25 eV are ∼2.5 eV wide, and the 5p bands broaden and mix with the $H_2-\sigma$ and H^-−bands. Core overlap forestalls the pressure-induced band-gap closure, which occurs at ∼100 GPa in our PBE calculations.

*P*4/*nmm* CsH_7 was found to be mechanically stable at 50 GPa, and the corresponding phonon densities of states is provided in Figure 2c. The peaks situated between 3500 and 4000 cm^{-1} result from the H_2 stretching modes. Since the intramolecular H−H bonds are somewhat elongated, compared to that of H_2 at 1 atm (0.75 Å), they are found at slightly lower frequencies compared to that of the free H_2 vibron (4161 cm^{-1}).[42]

■ H_3^- MOLECULES IN CsH_3

Five Unique Phases. Above 30 GPa, the CsH_3 stoichiometry has the most negative ΔH_F and it persists as the global minimum on the convex hull up to at least 150 GPa. Remarkably, an evolutionary search at 50 GPa uncovered five nearly isoenthalpic but distinct phases that did not exhibit any imaginary phonon modes. The zero-point energies (ZPEs) of these five phases differed by <1 meV/atom, and their inclusion did not affect the ordering of the relative enthalpies. The nearly equivalent ZPEs can be understood by noting that the phonon densities of states of the CsH_3 configurations, shown in the SI, all contained the same characteristic features.

At 30 GPa, the *Cmmm* structure was found to be favored; however, the enthalpies of the C_2c and $I4_1/amd$ configurations were only 2 meV/atom higher, as illustrated in Figure 3. Since the energy cutoff and *k*-point sampling were chosen such that the enthalpies were converged to within ∼1−2 meV/atom across the pressure range studied, this difference is within the precision of our calculations. The three phases are isoenthalpic at 40 GPa. Above this pressure, $I4_1/amd$ becomes the most stable structure and remains so until at least 200 GPa, with the *Cmmm* geometry consistently lagging behind by ∼2 meV/atom. In addition the P_2c, C_2c, and *Cmma* arrangements lie within 2−8 meV/atom of the most favorable structure within the 30−200 GPa pressure range.

Inclusion of finite temperature effects to the free energy at 50 GPa had very little influence on the relative stabilities of the five phases. The main difference was that at higher temperatures the *Cmma* structure became preferred over the P_2c. The free energies were employed to calculate the percentages of each phase present at 100 K, assuming a Boltzmann distribution;

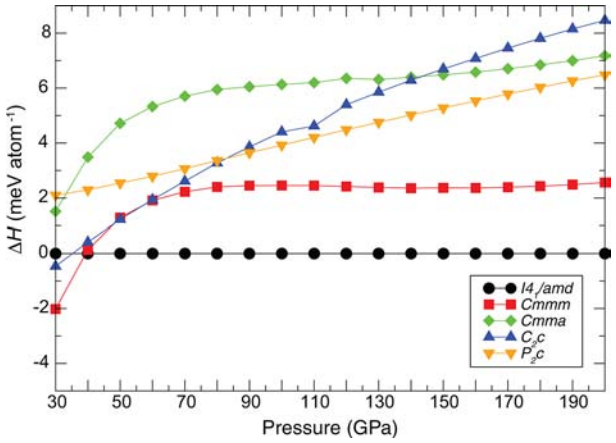

Figure 3. Relative enthalpies (ΔH) vs pressure for the five CsH_3 configurations, with respect to the $I4_1/amd$ structure. Inclusion of the zero-point energies (ZPEs) had a negligible affect on the relative enthalpies at 50 GPa.

these varied between 15% and 25%, with the $I4_1/amd$ structure being the most, and the *Cmma* structure the least abundant.

Evolutionary searches located similar stoichiometries and geometries for the potassium and rubidium polyhydrides as those found here. This is likely due to the congruent electronic structures of elemental K, Rb, and Cs, which all undergo a pressure-induced electronic s → d transition, and whose p semi-core levels hybridize with the valence d under further compression. For example, a KH_3 *C*2/*m* symmetry structure composed of K^+ cations and slightly bent H_3^- molecules was found to be metastable at pressures of ∼100 GPa.[31] But, the stability of KH_2 prevented this system from ever lying on the convex hull up to at least 250 GPa. For the rubidium polyhydrides, however, the RbH_3 stoichiometry was found to have the lowest ΔH_F above 220 GPa, at which point it underwent a pressure-induced structural phase transition from the $I4_1/amd$ configuration to the *Cmmm* configuration.[32] These RbH_3 systems are isostructural to the two most stable CsH_3 phases found throughout the pressure range considered here.

Each of the five CsH_3 structures consists of a Cs^+ cation and a symmetric, linear, H_3^- molecule—the simplest example of a three-centered four-electron bond. Whereas, in the gas phase, an asymmetric H_3^- with one short bond (0.752 Å) and one long bond (2.836 Å) is a shallow minimum on the potential energy surface,[43] it was previously demonstrated in our studies of the rubidium polyhydrides that under pressure symmetrization ensues due to the propensity of compressed systems to form electron-rich multicentered bonds. Moreover, since H_2 is an exceptionally weak electrophile, forcing it to bond with an H^- nucleophile to form H_3^- requires the presence of the softest, or most electropositive, alkali metal.[31] This helps explain why symmetric H_3^- motifs are evident in the preferred potassium and rubidium polyhydrides, but were not observed in any of the LiH_n or NaH_n ($n > 1$) species found in our evolutionary structure searches. Similar to how RbH_5 (which consisted of Rb^+, H_3^-, and H_2) becomes the global minimum on the convex hull near 16 GPa,[32] the global stabilization of CsH_3 at 30 GPa correlates with the pressure-induced symmetrization of its constituent H_3^- molecules; below 30 GPa, the most stable CsH_3 configurations have asymmetric $H^-\cdots H_2$ units.

Layers of H_3^- Molecules and Cs^+ Cations. The similarity of the enthalpies of the five phases is suggestive of liquid-like

dx.doi.org/10.1021/ic301045v | *Inorg. Chem.* 2012, 51, 9333−9342

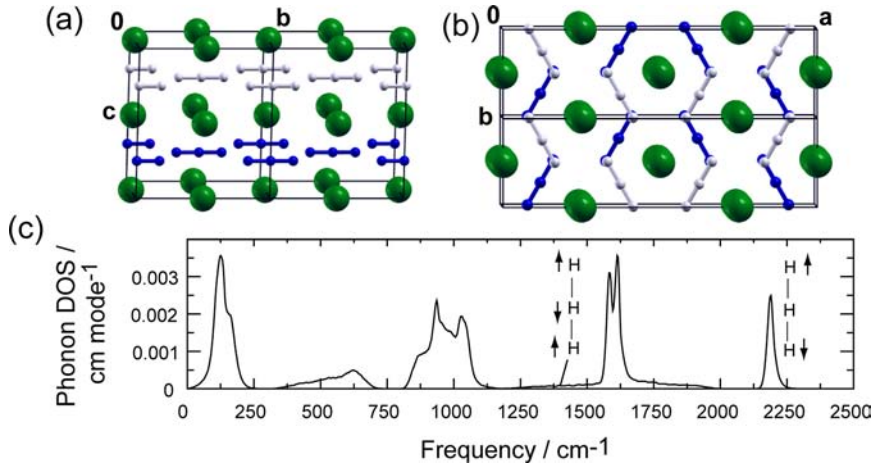

Figure 4. Supercells of the (a) *Cmmm* and (b) *Cmma*−CsH_3 structures. The H_3^- units in two different layers are highlighted by coloring one in blue and the other in white. (c) The phonon densities of states of *Cmmm* CsH_3 at 50 GPa. The modes corresponding to the symmetric and asymmetric stretch at the Γ-point of the H_3^- molecules are highlighted.

behavior of the hydrogenic sublattices, as has been proposed for other hydrogen-rich systems in combination with a heavy metal.[19,32] The Cs^+ sublattices from all five structures collectively belong to one of two different spacegroups: the *Cmmm* and *Cmma* arrangements have a *Cmmm* symmetry Cs^+ sublattice, while for the C_2c, $I4_1/amd$, and P_2c geometries, it is roughly of $I4_1/amd$ symmetry. This structural similarity suggests the possibility of liquid-like behavior under pressure, but our explorations of plausible pathways by which the *Cmmm* and *Cmma* structures could interconvert were found to have very high energy barriers.

Actually, it was possible to subdivide the five phases into these same groups based on whether the H atoms and Cs^+ cations formed separate layers (*Cmmm* and *Cmma*), or whether they did not ($I4_1/amd$, P_2c, and C_2c). By separate layers, we mean two parallel planes which contained either all of the Cs or all of the H atoms. As will be illustrated below, the layering and the corresponding orientations of the H_3^- molecules along these layers is found to have a profound impact on the electronic structures of these phases.

The *Cmmm* geometry, illustrated in Figure 4a, is the simplest of all the CsH_3 structures. The Cs^+ cations form a slightly distorted triangular two-dimensional lattice and are arranged in an AAA-type stacking. Falling between these are layers of H_3^- molecules. At 100 GPa, the distances between the Cs^+ cations in a single layer are 3.080, 3.080, and 3.146 Å, which is comparable to the distance between layers, 3.069 Å. The intramolecular H−H distances measure 0.931 Å and the shortest intermolecular distance is nearly twice as long (1.758 Å). This configuration was found to have the lowest enthalpy of any of the CsH_3 structures below 40 GPa: the pressure at which band-gap closure occurs at the PBE level of theory. The phonon density of states of *Cmmm* CsH_3 at 50 GPa in Figure 4c is representative of the other four phases (whose phonon DOS is given in the SI). The first peak in the doublet at ∼1600 cm^{-1} corresponds to the bending of the H_3^- units into the Cs^+ layers, whereas the second peak is a bending within the layers. These values match well with those calculated for the bending modes of various RbH_3 configurations at pressures of 150−220 GPa. The symmetric and asymmetric stretching modes of the H_3^- molecules are the sharp peak at ∼2100 cm^{-1}, and the peak which disperses from 1400 cm^{-1} to 1800 cm^{-1}. These are found at slightly lower frequencies than in RbH_3 (between 2200 and 3000 cm^{-1}) because of the fact that, at 50 GPa in CsH_3, the H_3^- molecules measure 0.963 Å and, at 150 GPa, they are compressed to 0.898 Å in RbH_3. These modes could be employed as a spectroscopic fingerprint to characterize CsH_3, if it should ever be made.

The *Cmma* structure (Figure 4b) is closely related to the *Cmmm* because it contains distinct layers of Cs^+ cations and H_3^- molecules. It may be obtained from the *Cmmm* by quadrupling the number of atoms in the primitive unit cell and rotating four H_3^- molecules by 120°. Because of this rotation, within a single layer, every row of H_3^- units is surrounded by two others: one that lays parallel to the first, and the second which is rotated so that it forms a herringbone-type arrangement. There is also a rotation of the H_3^- molecules by 60° in two adjacent layers, so that they form an ABABA... stacking. At 100 GPa, the intramolecular H−H distances are the same as in the *Cmmm* arrangement, the shortest intermolecular distances within a row measure 1.786 Å, and 3.079 Å between rows. Despite the structural similarity between the *Cmmm* and *Cmma* structures, a facile interconversion between them cannot occur. During the rotation, the terminal hydrogens in an H_3^- molecule would need to pass between two Cs^+ cations belonging to different layers. At 50 GPa, the distance between the Cs atoms is only 3.25 Å, and the rotation barrier we calculate is 7 eV per H_3^- molecule, which is significantly higher than the thermal energy at room temperature. This very large barrier is likely a result of the close proximity of the H atoms to the Cs, which decreases from ∼2.3 Å to roughly the ionic radius of Cs^+ (1.6 Å) during the rotation. This results in the H_3^- molecule being over an angstrom closer to the Cs atom than in CsH, which has an interatomic distance of 2.5 Å at 50 GPa. At the PBE level of theory, *Cmma* CsH_3 undergoes pressure-induced band gap closure at 50 GPa, comparable to the pressure calculated for the metallization of *Cmmm* CsH_3.

Building Blocks Composed of Triangular Prisms. The other three CsH_3 phases uncovered by our evolutionary runs did not become metallic below 200 GPa in the PBE calculations. Above 40 GPa, the $I4_1/amd$ structure exhibited the lowest enthalpy of any of the CsH_3 structures considered; it undergoes pressure-induced band gap closure at 220 GPa within PBE. The P_2c geometry was found to metallize at ∼320 GPa. The C_2c structure remains insulating until pressures well

dx.doi.org/10.1021/ic301045v | *Inorg. Chem.* 2012, 51, 9333−9342

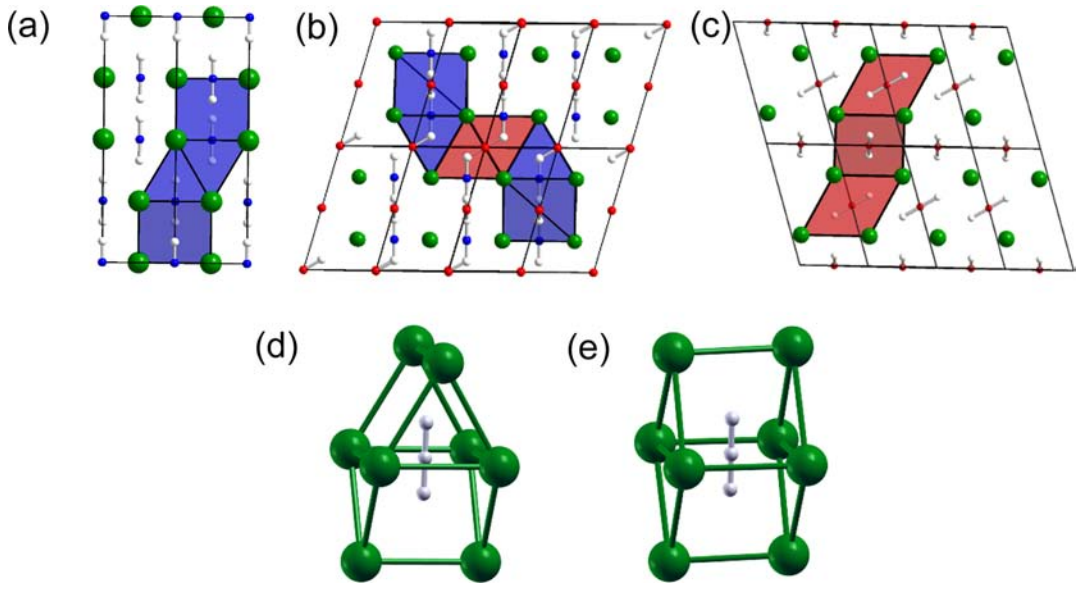

Figure 5. Supercells of the (a) $I4_1/amd$, (b) P_2c, and (c) C_2c CsH_3 phases. The building blocks which constitute these structures are colored as blue (d) and red (e).

above 350 GPa, at which point the PBE band gap is still 0.64 eV.

The perspectives of the structures of the nonlayered systems shown in Figures 5a–c illustrate the same axial projection of the Cs^+ sublattice—which is common to all three configurations. Barring minor structural distortions, these phases differ mostly in how the H_3^- are spread about the lattice. We find the H_3^- molecules to be surrounded by one of two distinct chemical environments. The two "building blocks" of the CsH_3 phases (see Figures 5d and 5e) are themselves composed of two fused triangular prisms of Cs atoms, with the H_3^- bisecting the common face. In the component shown in Figure 5e, a mirror plane of symmetry passes through this face, whereas the unit illustrated in Figure 5d contains an S_2 improper axis of rotation. The types and tilings of these building blocks define the structure. For example, the $I4_1/amd$ geometry exclusively uses the constituent from Figure 5d (see Figure 5a), and the blocks are arranged such that the H_3^- molecules are all aligned in the same direction. The C_2c geometry, on the other hand, consists of a periodic arrangement of units from Figure 5e; the faces of three adjoining building blocks are colored red in Figure 5c to show the two possible orientations the building blocks adopt. The P_2c structure is the only one of the three to use both polyhedra in a 1:1 ratio, as colored in Figure 5b, giving rise to its more-complex appearance.

In fact, the *Cmmm* and *Cmma* structures are related to the C_2c, as they can also be built from a tiling of the block shown in Figure 5(e). A similarity arises between the lowest enthalpy *Cmmm* and $I4_1/amd$ structures; they adopt tilings in which the H_3^- molecules are all aligned parallel to each other. In the case of the $I4_1/amd$, this requires a 90° rotation of every second building block which shares a face with another and prevents the formation of H_3^- and Cs layers throughout the crystal structure like those present in the *Cmmm*. In the *Cmma* geometry, the stacking of the building blocks creates a herringbone effect with respect to the positions of the H_3^- molecules (see Figure 4b), but still allows the hydrogens to remain in the same plane of the crystal.

Three-Connected Nets of H_3^- Molecules. Elemental cesium undergoes a pressure-induced electronic s → d transition,[44,45] so that Cs is essentially a d^1 metal by 15 GPa.[46] This electronic transition leads to an intriguing sequence of phase transitions. At 2.3 GPa, bcc-Cs transforms to a face-centered cubic (fcc) phase;[47] a complicated structure with 84 atoms in the unit cell is found between ~4.2–4.3 GPa;[48] and at 4.3 GPa, Cs-III transitions into the non-close-packed tetragonal Cs-IV,[49] which metamorphoses into orthorhombic Cs-V at 12 GPa.[50] Finally, at 70 GPa, Cs–VI once again assumes a close-packed structure, in which the 5p semi-core levels hybridize with the 6d.[51] In the vicinity of the Cs-IV → Cs-V transition, superconductivity is observed below 1.5 K.[52]

Because of the pressure-induced s → d transition, the maximum electron density in Cs-IV is found in the interstitial regions. It has been pointed out that this electron density can be reconstructed from the one calculated for Cs-II by periodic displacements of the 2D square nets.[53] The Cs atoms in Cs-IV are found in the same positions as the Th atoms in α-$ThSi_2$, and the maximum of electron density for both structures is located along zigzag chains, which correspond to empty regions in the former structure, and Si atoms in the latter. Because of this von Schnering and Nesper proposed that Cs-IV can be thought of as an electride, Cs^+e^-, where, on average, one electron occupies the position of two Si atoms in α-$ThSi_2$.[35] $ThSi_2$ is dimorphic and can be found in one of two structures, depending on the temperature of preparation.[54] The high-temperature allotrope, β-$ThSi_2$, possesses the AlB_2 structure in which the silicon sublattice forms a honeycomb network, and the Th atoms adopt triangular layers.

Curiously, the Cs^+ cations in the *Cmmm* and $I4_1/amd$ CsH_3 phases are found in exactly the same locations as the Th atoms in β-$ThSi_2$ and α-$ThSi_2$,[55] respectively, and the hydrogenic sublattices strongly resemble the Si three-connected nets. However, whereas in the β-allotrope, the Si net is hexagonal, in *Cmmm* CsH_3, two H_3 molecules comprise the long parallel edges of a slightly elongated hexagon, and the four nearest-neighbor intermolecular contacts comprise the short edges, as

dx.doi.org/10.1021/ic301045v | Inorg. Chem. 2012, 51, 9333–9342

illustrated in Figure 6b. At 100 GPa, the long and short edges of the hexagon measure 1.862 and 1.758 Å, respectively. Similarly,

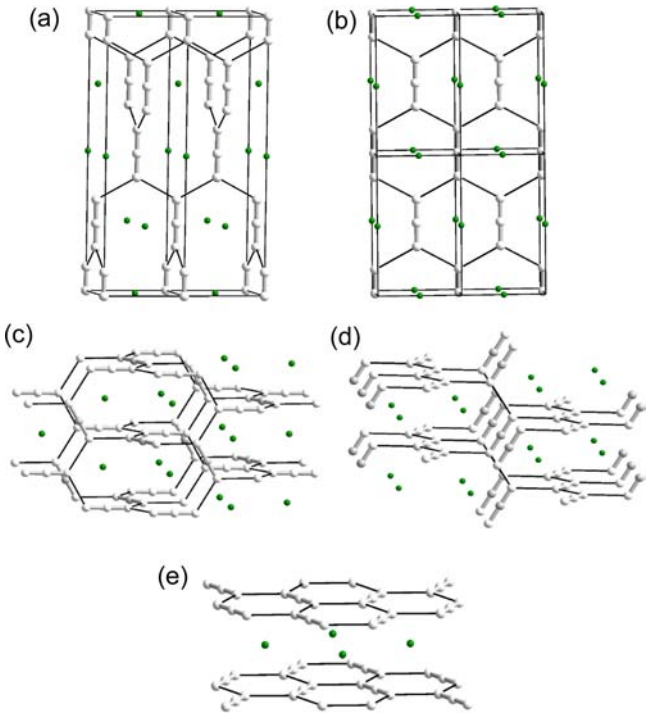

Figure 6. The hydrogenic sublattices of the (a) $I4_1/amd$, (b) *Cmmm*, (c) P_2c, (d) C_2c, and (e) *Cmma* CsH_3 geometries, drawn to highlight their structural similarity to the Si three-connected nets found in (a, c, d) α-$ThSi_2$ and (b, e) β-$ThSi_2$ structures. The positions of the Cs atoms, H_3^- molecules, and H−H closest intermolecular contacts are labeled in green, white, and black, respectively.

the twisted silicon net in the α-allotrope is congruent to the hydrogenic sublattice in $I4_1/amd$ CsH_3, where the H_3^- molecules are positioned akin to the parallel pairs of Si atoms (see Figure 6a). At 100 GPa, the H_3^- units measure 1.866 Å, and the shortest distance between them is 1.736 Å.

In fact, closer examination of the hydrogenic sublattices of the five CsH_3 structures shows that they correspond either to the Si three-connected net of α-$ThSi_2$ ($I4_1/amd$, P_2c, and C_2c) or β-$ThSi_2$ (*Cmmm* and *Cmma*). The only difference between the members of each set is the way in which the H_3^- molecules are arranged (see Figure 6). In the *Cmmm* and $I4_1/amd$ structures, they are parallel to each other, so the Cs^+ sublattice is able to maintain the symmetry of the thorium network in $ThSi_2$. In *Cmma*, C_2c, and P_2c, the H_3^- molecules are no longer parallel, leading to a slight distortion of the Cs^+ sublattice from the ideal.

Actually, when the H atoms were removed from the CsH_3 geometries, which were subsequently optimized at 12 GPa, the C_2c, P_2c, and $I4_1/amd$ sublattices yielded the same Cs-IV structure, whereas the *Cmmm* and the *Cmma* produced another. The latter has $P6/mmm$ symmetry and is 36 meV/atom less stable than Cs-IV; phonon calculations show that it is not mechanically stable. At 50 GPa, the first and second nearest-neighbor Cs−Cs distances in the five CsH_3 structures, which ranged from 3.229 to 3.353 Å, matched up well with those calculated for the elemental Cs-IV and the $P6/mmm$ phase at 12 GPa: 3.309−3.498 Å and 3.265−3.556 Å, respectively. Importantly, the maximum of the electron density calculated for the $P6/mmm$ and $I4_1/amd$ elemental Cs lattices is found in exactly the same region as the H_3^- sublattice in the five CsH_3 phases uncovered in this work.

Thus, the stability of the CsH_3 structures found in our evolutionary runs can be understood by considering the following. In $I4_1/amd$, C_2c, and P_2c CsH_3, the Cs^+ cations adopt the Cs-IV structure, whereas the H_3^- molecules occupy the regions of maximum electron density. However, there is more than one distinct way to distribute the H_3^- so that a twisted three-connected net is formed. The arrangement in the C_2c and P_2c structures breaks the symmetry; as a result, the Cs atoms optimize to a position deviating slightly from those in the ideal $I4_1/amd$ structure. A similar reasoning can be used to describe the formation of the *Cmmm* and *Cmma* configurations, except the underlying Cs sublattice is not the thermodynamic minimum at pressures that would yield approximately the same Cs−Cs distances as those found in the polyhydride. It may be that, at higher pressures, the most-stable CsH_3 phases adopt structures where the Cs^+ ions lay in the position of the Cs atoms in Cs-V or Cs-VI, and the H_3^- units are squeezed in the interstitial regions in which the valence electron density resides.

Pressing on to Metallization. The PBE electronic densities of states (DOS) of the five phases at select pressures are provided in Figure 7. The structures that contained layers of

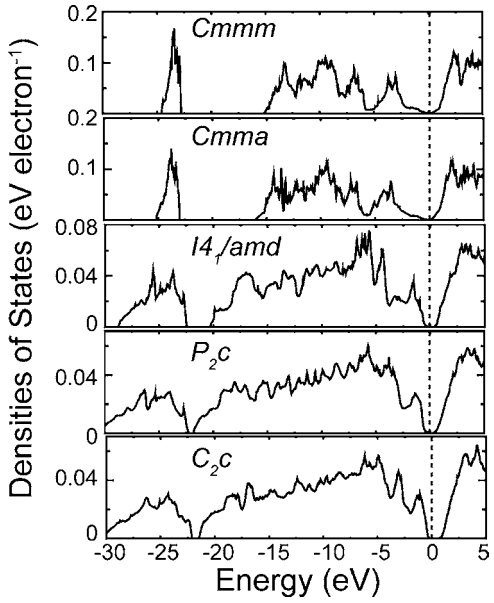

Figure 7. The PBE electronic DOS of *Cmmm*, *Cmma*, $I4_1/amd$, and P_2c CsH_3 near their PBE metallization pressures of 40, 50, 220, and 320 GPa. The lower panel shows the DOS of the C_2c structure, which maintained a band gap of 0.64 eV, even at 320 GPa. The peaks near −25 eV correspond to the Cs 5s, whereas the 5p electrons hybridize with bands derived from the H_3^- bonding and nonbonding orbitals. The Fermi energy is set to zero.

Cs^+ cations and H_3^- molecules were found to be metallic at experimentally achievable pressures, whereas the C_2c, P_2c, and $I4_1/amd$ phases required at least four times the pressure in order for band-gap closure to occur. For the *Cmmm* and *Cmma* phases, calculations were also carried out using the HSE06 hybrid functional[56] (see the SI), which has been shown to provide more-accurate band gaps in solids. Indeed, these two CsH_3 configurations were shown to have a small, but finite, DOS at the Fermi level at 80 and 100 GPa, respectively. GW

dx.doi.org/10.1021/ic301045v | *Inorg. Chem.* 2012, 51, 9333−9342

calculations, which could verify the metallicity of these phases, are past the scope of the work presented here. The $I4_1/amd$ structure, which was computed to be metallic at 220 GPa via PBE, maintained a band gap of 0.59 eV at 250 GPa when the screened hybrid functional was employed. The DOS of the P_2c and C_2c phases were not recomputed, since band gap closure (within PBE) did not occur until pressures greater than 300 GPa.

Interestingly, single-point computations on the negatively charged hydrogenic sublattices at 100 GPa (where the Cs^+ had been removed) were all shown to be metallic, indicating that interaction with the metal cations had a profound impact on the electronic structure. Calculations on the neutral Cs sublattices showed that they also were metallic. In order to investigate why the two layered phases emerged as metallic in our calculations below pressures of 100 GPa, whereas the others did not, the band structures decorated with orthonormal LMTO characters (fat bands, see the SI) were calculated for *Cmmm*, *Cmma*, and $I4_1/amd$ CsH_3.

For all of these, the character of the bands around −25 eV (see Figure 8) displayed Cs 5s character. The bands between approximately −20 eV up to the Fermi level contained a substantial amount of Cs 5p character. The broadening of the Cs core bands is indicative of pronounced core overlap. Because of the pressure-induced s → d transition, the bands directly above the Fermi level contained a greater amount of Cs 5d character, rather than Cs 6s character. Of course, there were also contributions from H s-character below the Fermi level, indicative of substantial hybridization with the Cs 5p. In H_3^-, both the bonding and nonbonding molecular orbitals (MOs) are filled (Figure 9a), so the occupied bands closest to the Fermi level that exhibit H s-character are derived from the latter. The Wannier functions for the two bands falling directly below the Fermi level in the *Cmmm* and $I4_1/amd$ configurations, illustrated in Figures 9c and 9d, are indicative of strong hybridization between the H_3^- nonbonding MO and the Cs 5p.

The fat bands illustrate that the *Cmmm* and *Cmma* structures are metallic, because a band exhibiting H s-character rises above the Fermi level, and one displaying Cs d-character falls below the Fermi level. The Bloch function derived from the H_3^- orbital in *Cmmm* CsH_3 at $(0, 0, k_z)$ is illustrated in Figure 9b. At the Γ-point, it is antibonding along the H_3^- nearest-neighbor contacts in a single plane (1.758 Å), bonding to the second-nearest-neighbor interplanar contacts (3.146 Å), and bonding to those in the plane below or above it (3.069 Å). At the *Z*-point the nonbonding MO becomes antibonding along the *c*-axis. In part because of this, at 100 GPa, the H_3^- band is 1.18 eV higher in energy at *Z* than at Γ. A molecular calculation on two H_3^- fragments constrained to have the same length as the H_3^- units at 100 GPa, and a distance of 3.069 Å between them, showed that the energy difference between the in-phase and out-of-phase combinations of the nonbonding MO differed by only 0.4 eV, suggesting that the presence of the Cs^+ also destabilizes this band at *Z*. A band exhibiting primarily Cs $d_{x^2-y^2}$ character has a lower energy at the *T*-point than does the nonbonding H_3^- band at the *Z*-point, which is the reason why *Cmmm* CsH_3 is metallic, as illustrated in Figure 8a.

Cmma, which also consists of layers of H_3^- molecules parallel to each other, metallizes because the energy of a band at the *Z*-point which displays primarily Cs d_{xz}-character is lower than that of one with H s-character at *Y*. Extended Hückel calculations on the Si three-connected nets have shown that

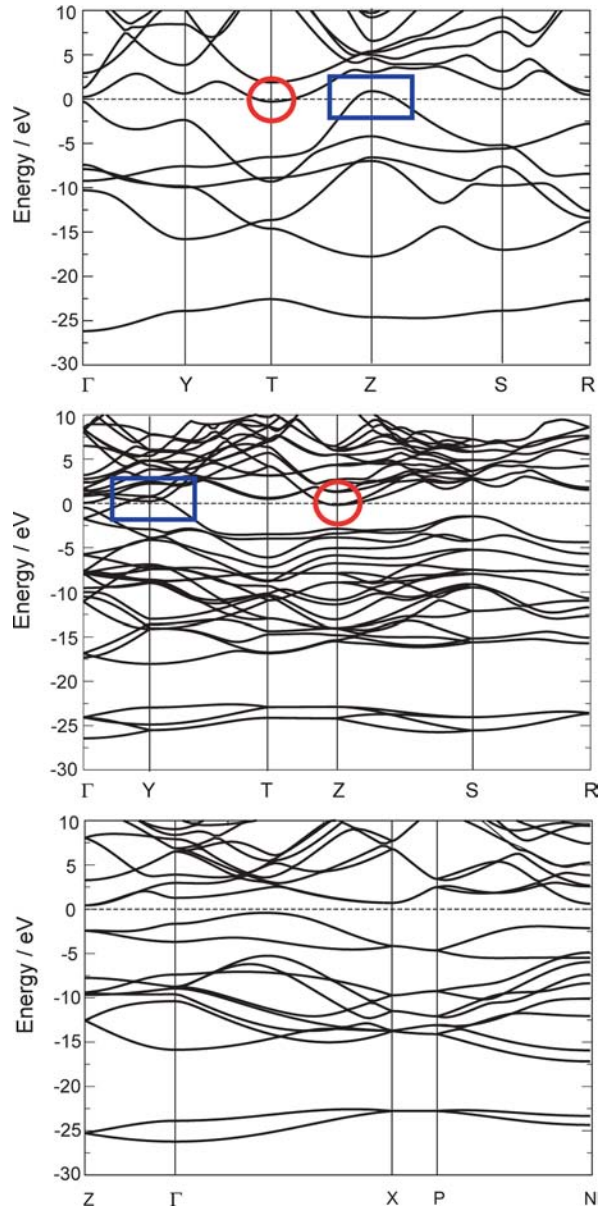

Figure 8. Band structures of the (top) *Cmmm*, (middle) *Cmma*, and (bottom) $I4_1/amd$ CsH_3 at 100 GPa. The blue boxes indicate bands that have primarily H s-character, and the red boxes denote bands with primarily Cs $d_{x^2-y^2}$-character (*Cmmm*), and Cs d_{xz}-character (*Cmma*).

the π- and π*-bands of the twisted structure are less disperse than that of the planar honeycomb lattice, so the former should be preferred over the latter when the electron count is such that doping into the π* band occurs.[57] We note that the dispersion of the H s-bands of the other three CsH_3 phases, whose hydrogenic sublattices correspond to the twisted Si net in α-$ThSi_2$, are ∼2 eV smaller than that of the layered structures at 100 GPa. As a result, metallization is not expected to occur in the twisted structures at pressures achievable in diamond anvil cells.

CONCLUSIONS

Evolutionary algorithms coupled with first-principles calculations have been employed to predict the structures of cesium polyhydrides under pressure. CsH_n with $n > 1$ starts to become stable, with respect to decomposition into CsH and H_2, at

dx.doi.org/10.1021/ic301045v | *Inorg. Chem.* 2012, 51, 9333−9342

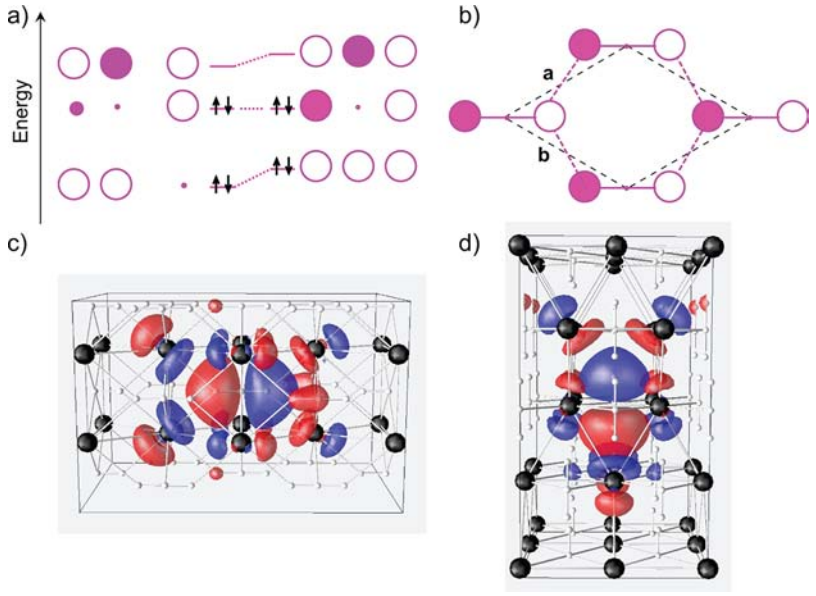

Figure 9. (a) Schematic illustration of an MO level diagram for an asymmetric and a symmetric H_3^- molecule showing the bonding, nonbonding, and antibonding MOs. (b) The Bloch function derived from the H_3^- nonbonding MO of *Cmmm* CsH_3 in the plane of the H atoms at (0, 0, k_z). When $k_z = 0$ (Γ-point), the Bloch function is bonding along the *c*-axis; when $k_z = \pi/c$ (*T*-point), it is antibonding. The pink dotted lines outline the nearest-neighbor intermolecular contacts, highlighting the slightly distorted hexagons comprising the hydrogenic sublattice. The H_3^- Wannier Functions (isovalue ±0.03 au) obtained from a basis which yielded the two bands directly below the Fermi level in the (c) *Cmmm* and (d) $I4_1/amd$ CsH_3 phases at 80 GPa.

pressures as low as 2 GPa. CsH_3, consisting of Cs^+ cations and H_3^- molecules, and CsH_7 with Cs^+ cations, H_2 molecules, and H^- units, were found to be thermodynamically stable up to at least 150 GPa. Phonon calculations revealed characteristic H_2 stretching, and H_3^- bending and stretching modes, which could be used as spectroscopic fingerprints to identify these species.

Remarkably, five distinct, mechanically stable, nearly isoenthalpic CsH_3 phases were uncovered by evolutionary searches at 50 GPa. Between pressures of 30−200 GPa, this stoichiometry is the global minimum on the convex hull. The Cs^+ and H_3^- sublattices of the five CsH_3 geometries could be traced back to the Th sublattices and Si three-connected nets in α-$ThSi_2$ ($I4_1/amd$, P_2c, and C_2c) and β-$ThSi_2$ (*Cmmm* and *Cmma*), respectively. Despite the similarities between the structures in these two sets, a facile pathway for their interconversion could not be found. Interestingly, the Cs^+ cations in the most stable CsH_3 phase, $I4_1/amd$, are located in the same positions as the Cs atoms in Cs-IV, and the Cs−Cs distances in the former at 50 GPa correlate well with those in the latter at 12 GPa. The H_3^- molecules, on the other hand, reside in the interstitial regions where the maximum of valence electron density in Cs-IV is situated.

Only *Cmmm* and *Cmma* CsH_3, with planar honeycomb-like hydrogenic nets, were computed to undergo pressure-induced metallization at pressures below 100 GPa (using the HSE06 screened hybrid functional). The $I4_1/amd$, P_2c, and C_2c arrangements, where the H_3^- nets are twisted, did not metallize until pressures greater than 300 GPa. The metallization of the two layered phases could be traced back to the geometries of the hydrogenic sublattices and the concomitant broadening of the bands derived from the H_3^- bonding and nonbonding MOs. In the *Cmmm* and *Cmma* phases, these bands were ∼2 eV wider at 100 GPa than in the other three structures; as a result, the top of the H_3^- nonbonding band was higher in energy than the bottom of a band exhibiting Cs d-character, so that the former fell above and the latter below the Fermi level.

■ COMPUTATIONAL DETAILS

The structural searches utilized the open-source evolutionary algorithm (EA) XtalOpt Release 7[34] and the parameter set suggested in ref 33. EA searches were carried out on unit cells containing up to four CsH_n formula units for $2 < n < 5$ and two formula units for $n > 5$ at 50 GPa—the pressure at which the cesium polyhydrides begin to metallize in our PBE calculations. At 2 GPa, further searches were carried out on CsH_3 and CsH_7, and the most stable structures found verified that as the pressure is released the H_3^- are likely to form asymmetric $H^-\cdots H_2$ motifs. Duplicates were detected using the XtalComp algorithm.[58] For each stoichiometry, the geometries of the lowest enthalpy structures were relaxed in the pressure range of 0.8−250 GPa.

Geometry optimizations and electronic structure calculations were performed using density functional theory (DFT) as implemented in the Vienna Ab Initio Simulation Package (VASP) version 4.6.31.[59] The projector augmented wave (PAW) method[60] was used to treat the core states, and a plane-wave basis set with an energy cutoff of 500 eV was utilized in the structural searches, and 600 eV otherwise. The Cs *5s*/*5p*/*6s* electrons were treated explicitly as valence electrons in all of the calculations. The gradient-corrected exchange and correlation functional of Perdew−Burke−Ernzerhof (PBE)[61] was adopted, and the *k*-point grids were generated using the Γ-centered Monkhorst−Pack scheme. The number of divisions along each reciprocal lattice vector was chosen such that the product of this number with the real lattice constant was 20 Å in the structural searches and 40 Å otherwise. In order to obtain a more accurate estimate of the pressure at which the *Cmmm*, *Cmma*, and $I4_1/amd$ CsH_3 phases metallize, their density of states (DOS) values were calculated using the HSE06 hybrid functional[56] at 80, 100, and 250 GPa, respectively.

Phonons and thermodynamic properties of selected CsH_3 and CsH_7 phases were calculated using the PHON package.[62] The supercells used for the phonon calculations were chosen such that the number of atoms in the simulation cell was between 108 and 216 for the various CsH_3 phases, and 432 for CsH_7.

dx.doi.org/10.1021/ic301045v | *Inorg. Chem.* 2012, 51, 9333−9342

The band structures of *Cmmm*, *Cmma*, and $I4_1/amd$ CsH_3 were calculated using the tight-binding linear muffin-tin orbital (TB-LMTO) method.[63,64] The VWN[65] local exchange correlation potential was used along with the Perdew–Wang[66] generalized gradient approximation, and scalar relativistic effects were included. The structural parameters of the CsH_3 phases were taken from those optimized with VASP at 80 GPa, and the band structures agreed well with those calculated using plane waves. The energy bands with orthogonal LMTO characters (fat bands) are provided in the SI. The NMTO method was employed to generate Wannier functions corresponding to the H_3^- nonbonding band, according to the procedure outlined previously in ref 32.

■ ASSOCIATED CONTENT

Supporting Information

Optimized coordinates, phonon density of states, site-projected densities of states, electronic densities of states obtained using the HSE06 hybrid functional, LMTO and *N*MTO band structures, and relative enthalpies of the cesium polyhydrides up to 200 GPa. This material is available free of charge via the Internet at http://pubs.acs.org.

■ AUTHOR INFORMATION

Corresponding Author

*E-mail: ezurek@buffalo.edu.

Notes

The authors declare no competing financial interest.

■ ACKNOWLEDGMENTS

We acknowledge the National Science Foundation (NSF) (No. DMR-1005413) for financial support, and the Center for Computational Research at SUNY Buffalo for computational support.

■ REFERENCES

(1) Narayana, C.; Luo, H.; Orloff, J.; Ruoff, A. L. *Nature* **1998**, *393*, 46–49.
(2) Loubeyre, P.; Occelli, F.; LeToullec, R. *Nature* **2002**, *416*, 613–617.
(3) Eremets, M. I.; Troyan, I. A. *Nat. Mater.* **2011**, *10*, 927–931.
(4) Howie, R. T.; Guillaume, C. L.; Scheler, T.; Goncharov, A. F.; Gregoryanz, E. *Phys. Rev. Lett.* **2012**, *108*, 125501-1–125501-5.
(5) Nellis, W. J.; Ruoff, A. L.; Silvera, I. F. *arXiv.org, E-Print Arch., Condens. Matter***2012**, arXiv:1201.0407v1.
(6) Lathiotakis, N. N.; Marques, M. A. L.; Lüders, M.; Fast, L.; Gross, E. K. U. *Int. J. Quantum Chem.* **2004**, *99*, 790–797.
(7) Pickard, C. J.; Needs, R. J. *Nat. Phys.* **2007**, *3*, 473–476.
(8) Cudazzo, P.; Profeta, G.; Sanna, A.; Floris, A.; Continenza, A.; Massidda, S.; Gross, E. K. U. *Phys. Rev. Lett.* **2008**, *100*, 257001-1–257001-4.
(9) McMahon, J. M.; Ceperley, D. M. *Phys. Rev. Lett.* **2011**, *106*, 165302-1–165302-4.
(10) McMahon, J. M.; Ceperley, D. M. *Phys. Rev. B* **2011**, *84*, 144515-1–144515-8.
(11) Wang, Y.; Lv, J.; Zhu, L.; Ma, Y. *Phys. Rev. B* **2010**, *82*, 094116-1–094116-4.
(12) Liu, H.; Wang, H.; Ma, Y. *J. Phys. Chem. C* **2012**, *116*, 9221–9226.
(13) Carlsson, A. E.; Ashcroft, N. W. *Phys. Rev. Lett.* **1983**, *50*, 1305–1308.
(14) Ashcroft, N. W. *Phys. Rev. Lett.* **2004**, *92*, 187002-1–187002-4.
(15) Klug, D. D.; Yao, Y. *Phys. Chem. Chem. Phys.* **2011**, *13*, 16999–17006.
(16) Gao, G.; Oganov, A. R.; Bergara, A.; Martinez-Canales, M.; Cui, T.; Iitaka, T.; Ma, Y.; Zou, G. *Phys. Rev. Lett.* **2008**, *101*, 107002-1–107002-4.
(17) Gao, G.; Oganov, A. R.; Li, P.; Li, Z.; Wang, H.; Cui, T.; Ma, Y.; Bergara, A.; Lyakhov, A. O.; Iitaka, T.; Zou, G. *Proc. Nat. Acad. Sci. U.S.A.* **2010**, *107*, 1317–1320.
(18) Tse, J. S.; Yao, Y.; Tanaka, K. *Phys. Rev. Lett.* **2007**, *98*, 117004-1–117004-4.
(19) Zaleski-Ejgierd, P.; Hoffmann, R.; Ashcroft, N. W. *Phys. Rev. Lett.* **2011**, *107*, 037002.
(20) Gao, G.; Wang, H.; Bergara, A.; Li, Y.; Liu, G.; Ma, Y. *Phys. Rev. B* **2011**, *84*, 064118.
(21) Wang, H.; Tse, J. S.; Tanaka, K.; Iitaka, T.; Ma, Y. *Proc. Natl. Acad. Sci. U.S.A.* **2012**, *109*, 6463–6466.
(22) Kim, D. K.; Scheicher, R. H.; Mao, H. K.; Kang, T. W.; Ahuja, R. *Proc. Natl. Acad. Sci. U.S.A.* **2010**, *107*, 2793–2796.
(23) Somayazulu, M.; Dera, P.; Goncharov, A. F.; Gramsch, S. A.; Liermann, P.; Yang, W.; Liu, Z.; Mao, H. K.; Hemley, R. J. *Nat. Chem.* **2010**, *2*, 50–53.
(24) Strobel, T. A.; Somayazulu, M.; Hemley, R. J. *Phys. Rev. Lett.* **2009**, *103*, 065701-1–065701-4.
(25) Wang, S.; Mao, H. K.; Chen, X. J.; Mao, W. L. *Proc. Nat. Acad. Sci. U.S.A.* **2009**, *106*, 14763–14767.
(26) Li, Y.; Gao, G.; Xie, Y.; Ma, Y.; Cui, T.; Zou, G. *Proc. Natl. Acad. Sci. U.S.A.* **2010**, *107*, 15708–15711.
(27) Li, Y.; Gao, G.; Li, Q.; Ma, Y.; Zou, G. *Phys. Rev. B* **2010**, *86*, 052101-1–052101-6.
(28) Strobel, T. A.; Ganesh, P.; Somayazulu, M.; Kent, P. R. C.; Hemley, R. J. *Phys. Rev. Lett.* **2011**, *107*, 255503-1–255503-4.
(29) Zurek, E.; Hoffmann, R.; Ashcroft, N. W.; Oganov, A. R.; Lyakhov, A. O. *Proc. Natl. Acad. Sci. U.S.A.* **2009**, *106*, 17640–17643.
(30) Baettig, P.; Zurek, E. *Phys. Rev. Lett.* **2011**, *106*, 237002-1–237002-4.
(31) Hooper, J.; Zurek, E. *J. Phys. Chem. C* **2012**, *116*, 13322–13328.
(32) Hooper, J.; Zurek, E. *Chem.—Eur. J.* **2012**, *18*, 5013–5021.
(33) Lonie, D. C.; Zurek, E. *Comput. Phys. Commun.* **2011**, *182*, 372–387.
(34) Lonie, D. C.; Zurek, E. *Comput. Phys. Commun.* **2011**, *182*, 2305–2306.
(35) von Schnering, H. G.; Nesper, R. *Angew. Chem., Int. Ed.* **1987**, *26*, 1059–1080.
(36) Ahuja, R.; Eriksson, O.; Johansson, B. *Physica B* **1999**, *265*, 87–91.
(37) Hooper, J.; Baettig, P.; Zurek, E. *J. Appl. Phys.* **2012**, *111*, 112611.
(38) Trimarchi, G.; Freeman, A. J.; Zunger, A. *Phys. Rev. B* **2009**, *80*, 092101-1–092101-4.
(39) Zhang, X.; Zunger, A. *Phys. Rev. Lett.* **2010**, *104*, 245501.
(40) Hooper, J.; Zurek, E. *ChemPlusChem* **2012**, DOI: 10.1002/cplu.201200130.
(41) Tse, J. S.; Frapper, G.; Ker, A.; Rousseau, R.; Klug, D. D. *Phys. Rev. Lett.* **1999**, *82*, 4472–4475.
(42) Stoicheff, B. P. *Can. J. Phys.* **1957**, *35*, 730.
(43) Ayouz, M.; Dulieu, O.; Guerout, R.; Robert, J.; Kokoouline, V. *J. Chem. Phys.* **2010**, *132*, 194309-1–194309-11.
(44) Sternheimer, R. *Phys. Rev.* **1950**, *78*, 235–243.
(45) Zurek, E.; Jepsen, O.; Andersen, O. K. *ChemPhysChem* **2005**, *6*, 1934–1942.
(46) McMahan, A. *Phys. Rev. B* **1984**, *29*, 5982.
(47) Hall, H. T.; Merrill, L.; Barnett, J. D. *Science* **1964**, *146*, 1297–1299.
(48) McMahon, M. I.; Nelmes, R. J.; Rekhi, S. *Phys. Rev. Lett.* **2001**, *87*, 255502 (1–4).
(49) Takemura, K.; Minomura, S.; Shimomura, O. *Phys. Rev. Lett.* **1982**, *49*, 1772–1775.
(50) Schwarz, U.; Takemura, K.; Hanfland, M.; Syassen, K. *Phys. Rev. Lett.* **1998**, *81*, 2711–2714.
(51) Takemura, K.; Christensen, N. E.; Novikov, D. L.; Syassen, K.; Schwarz, U.; Hanfland, M. *Phys. Rev. B* **2000**, *61*, 14399–14404.
(52) Wittig, J. *Phys. Rev. Lett.* **1970**, *24*, 812–815.
(53) Tse, J. S. *Z. Kristallogr.* **2005**, *220*, 521–530.

(54) Jacobson, E. L.; Freeman, R. D.; Tharp, A. G.; Searcy, A. W. *J. Am. Chem. Soc.* **1956**, *78*, 4850−4852.
(55) Zurek, E.; Jepsen, O.; Andersen, O. K. *Inorg. Chem.* **2010**, *49*, 1384−1396.
(56) Krukau, A. V.; Vydrov, O. A.; Izmaylov, A. F.; Scuseria, G. E. *J. Chem. Phys.* **2006**, *125*, 224106.
(57) Zheng, C.; Hoffmann, R. *Inorg. Chem.* **1989**, *28*, 1074−1080.
(58) Lonie, D. C.; Zurek, E. *Comput. Phys. Commun.* **2012**, *183*, 690.
(59) Kresse, G.; Hafner, J. *Phys. Rev. B* **1993**, *47*, 558−561.
(60) Blöchl, P. *Phys. Rev. B* **1994**, *50*, 17953.
(61) Perdew, J. P.; Burke, K.; Ernzerhof, M. *Phys. Rev. Lett.* **1996**, *77*, 3865−3868.
(62) Alfè, D.; Price, G. D.; Gillan, M. J. *Phys. Rev. B* **2001**, *64*, 045123.
(63) Andersen, O. K. *Phys. Rev. B* **1975**, *12*, 3060.
(64) Andersen, O. K.; Jepsen, O. *Phys. Rev. Lett.* **1984**, *53*, 2571.
(65) Vosko, S. H.; Wilk, L.; Nusair, M. *Can. J. Phys.* **1980**, *58*, 1200.
(66) Perdew, J. P.; Wang, Y. *Phys. Rev. B* **1986**, *33*, 8800.